

A VIMOS spectroscopy of photometric variables and straggler candidates in ω Centauri \star

M. Rozycka¹, J. Kaluzny¹, P. Pietrukowicz^{1,2}, W. Pych¹, M. Catelan², and C. Contreras²

¹ Nicolaus Copernicus Astronomical Center, ul. Bartycka 18, 00-716 Warszawa, Poland

² Pontificia Universidad Católica de Chile, Departamento de Astronomía y Astrofísica, Av. Vicuña MacKenna 4860, 782-0436 Macul, Santiago, Chile

Received ...; accepted ...

ABSTRACT

We report a spectroscopic study of 19 photometric variables and 55 blue, yellow and red straggler candidates in the field of ω Centauri. We confirm the cluster membership of 18 variables and 54 straggler candidates. Velocity variations are detected in 22 objects, and another 17 objects are classified as suspected of being velocity-variable. Velocity data of 11 photometric variables phase with their photometric periods, however none of these objects has a mass function indicating the presence of a massive degenerate component. Based on both photometric and spectroscopic data we find that the fraction of binaries among blue stragglers may be as high as 69 per cent.

Key words. globular clusters: individual: NGC 5139 (ω Centauri) – binaries: close – binaries: spectroscopic – blue stragglers – red stragglers

1. Introduction

Globular clusters harbor a massive population of close binary systems with degenerate components (hereafter referred to as degenerate binaries), discovered primarily due to their X-ray emission (e.g. Pooley 2010, and references therein). Unfortunately, detailed studies of these interesting objects are hampered by the fact that their optical counterparts are often weak and hard to identify in the crowded environment (Verbunt et al. 2008, e.g.). On the other hand, many field X-ray binaries exhibit long periods of quiescence. The nature of a quiescent binary is betrayed by a low-amplitude optical modulation induced primarily by the ellipsoidal effect from the nondegenerate component, while a spectroscopic observer would see it as a single-line system with large orbital velocity ($K > 150 \text{ km s}^{-1}$). Perhaps the best examples of such objects are X-ray novae which almost certainly harbor black holes. They would be distinguished by a mass function $f_m = (m \sin i)^3 / (m_{bin})^2 > 2M_\odot$, where m and m_{bin} stand, respectively, for the mass of the degenerate component and the total mass of the binary (Remillard & McClintock 2006).

The first spectroscopic search for quiescent degenerate binaries in globular clusters was conducted by Rozycka et al. (2010) based on a sample of short-period, low-amplitude optical variables with nearly sinusoidal light curves and periods shorter than ~ 1.3 days. The sample included 4 objects from NGC 6397 and 7 objects from ω Centauri (NGC 5139). The most interesting findings were turnoff binaries V17 and V36 in NGC 6397, whose invisible primary components had masses larger than $1 M_\odot$ (in the case of V36 even larger than $2 M_\odot$, albeit with a large uncertainty). In the present paper we continue the search for degenerate binaries in ω Cen based on a sample of 20 optical variables with periods obtained by Kaluzny et al. (2004), which were clas-

sified by Bellini et al. (2009) as proper-motion members of that cluster.

Another class of cluster members certainly worth of spectroscopic investigation consists of objects populating “nonstandard” areas of the color-magnitude diagram (CMD): blue stragglers, yellow stragglers, and sub-subgiants (also called red stragglers; see e.g. Platais et al. 2011).

Blue stragglers were originally defined as stars located at the extension of the main sequence above the turnoff point. Being both brighter and hotter (“bluer”) than turnoff stars, they made an impression of evolving at a slower rate than normal cluster members. Although they have been known for almost 50 years (Sandage 1953), the mechanism of their formation remains controversial. The various possibilities include mass transfer between the components of a binary, merger of a binary or direct collision of stars. It is also conceivable that all these mechanisms are at work, perhaps with various relative efficiency in various clusters (Ferraro 2006; Ferraro et al. 2006; Dalessandro et al. 2008).

The results of Rozycka et al. (2010) point to an extensive mass exchange rather than stellar collisions, as in all cases they report the brighter component of the blue-straggler binary is the more massive primary star which must have acquired significant amounts of hydrogen-rich material from its companion. Thus, if their sample is representative, then many blue stragglers must be Algol-like systems in which the original mass ratio has been reversed, causing the mass transfer to effectively stop. One of the best studied blue stragglers, star V228 in 47 Tuc is indeed a classical Algol (Kaluzny et al. 2007b); however, in other cases the similarity to Algols may be purely morphological. A good example is the also well-studied star V209 in ω Cen, which most probably underwent two mass transfer episodes. Its present primary seems to be “reborn” from a former white dwarf that accreted a new envelope through mass transfer from its companion, while the present secondary lost most of its envelope during the ascent

\star Based on photometric data collected at Las Campanas Observatory, and spectroscopic data collected with the Very Large Telescope at European Southern Observatory (ESO programme 384.D-0736).

along the subgiant branch, failed to ignite helium, and is now powered by a hydrogen-burning shell (Kaluzny et al. 2007a).

Yellow stragglers reside in the area between the subgiant branch and the horizontal branch. Most probably, they are evolutionary advanced blue stragglers (e.g. Xin et al. 2011), and distinguishing between these two groups of objects seems to be a matter of taste rather than physical necessity. Red stragglers are found to the right of the main sequence, below the subgiant branch. They are even less explored than the blue ones, and the conundrums they pose are even more mysterious (Platais et al. 2011).

Both the degenerate binaries and all kinds of stragglers are thought to be products of the evolution of binary systems in a dense stellar environment, and their peculiarities are most probably promoted or even induced by interactions between cluster members (Ferraro 2006; Platais et al. 2011). As such, they provide a link between classical stellar evolution and dynamical evolution of the cluster, being a valuable observational template against which the dynamical models of stellar aggregates can be tested. The straggler-related goal of the present survey is to verify the membership of straggler candidates selected from the proper-motion catalogue of ω Cen by Bellini et al. (2009), and to establish how frequent binary systems are in the straggler population.

2. Observations and data reduction

We monitored selected targets in ω Cen with the help of VIMOS – a multi-purpose instrument mounted in the Nasmyth B focus of the ESO VLT-Unit 3 telescope. For the present survey it was working as a multi-object spectrograph. To adapt it to the observations of blue stragglers, we selected the HR blue mode with wavelength range 4100 – 6300 Å, resolution 2050 – 2550 (150 – 120 km s⁻¹) and dispersion 0.5 Å/pixel.

A VIMOS spectroscopy run consists of pre-imaging and spectroscopic follow-up. The pre-imaging frames of ω Cen were obtained on 2010.16.01 to serve as a basis for the preparation of masks with slits centered on objects chosen for the survey. The spectroscopic monitoring was performed during ten nights in February and March 2010. On every night one ~30 min observation was made, consisting of acquisition-imaging, two spectroscopic integrations of 580 sec. each, up to three flat-field exposures, and helium-neon lamp exposure for wavelength calibration. The VIMOS field of view, which is composed of four 7×8 arcmin quadrants served by independent CCDs and separated by about 2 arcmin gaps, was centered on $(\alpha, \delta)_{2000} = (13^{\text{h}}26^{\text{m}}46.3^{\text{s}}, -47^{\circ}27'51.8'')$. A log of the observations is presented in Table 1, in which date and airmass are given for the start of the exposures, and the seeing is averaged over each observation.

Table 1. Log of observations.

ID	UT date	Airmass	Seeing (arcsec)
1	2010 02 11.32	1.11	2.0
2	2010 02 12.32	1.11	1.5
3	2010 02 13.31	1.12	1.0
4	2010 02 14.30	1.14	1.0
5	2010 02 21.26	1.19	1.0
6	2010 02 22.30	1.11	0.7
7	2010 02 23.25	1.19	0.7
8	2010 03 09.38	1.21	1.0
9	2010 03 10.30	1.09	1.3
10	2010 03 12.24	1.11	0.7

The target objects were selected from variable star catalog of Kaluzny et al. (2004), henceforth identified by a number preceded with V or NV, and proper-motion catalog of Bellini et al. (2009), henceforth identified by a number preceded with B. We adopted the following selection criteria:

- $V < 19$ mag (assuming 1'' slit, 1'' seeing and reasonably long exposure of ~1000 s, this is the magnitude at which the S/N ratio expected for the latest spectral types in our sample amounts to ~20);
- Membership probability mp in Bellini et al. (2009) should be at least 90%;
- The image of the target should not blend with images of other objects on pre-imaging frames;
- The distribution of targets on pre-imaging frames should maximize the number of slits.

Photometrically detected pulsating stars, whose intrinsic variations of radial velocity could mask orbital effects, were excluded from the sample. The selection procedure was rather tedious, and trying to maximize the number of photometric variables in the sample we were forced to relax the second criterion. After a few trials we decided to focus on 81 objects: 61 straggler candidates and 20 photometric variables, among which NV332, NV334 and NV361 had membership probabilities equal to 84%, 88% and 64%, respectively. We deliberately included V209 – a system thoroughly investigated by Kaluzny et al. (2007a) – with the intention to use it as an indicator of the quality and reliability of velocity measurements. In the sample there are a few blue objects which, strictly speaking, do not conform to the classical definition of blue stragglers, because they are located not on the main-sequence extension, but to the left of it. We included them in order to maximize the total number of slits.

VIMOS spectra can be calibrated automatically by the ESO-VIMOS pipeline, which, however, cannot be 100% trusted. This is because the spectra of some slits extend below $\lambda = 5000$ Å, where calibration lamp lines are scarce (ESO 2011), and some of them are very weak. While Giuffrida et al. (2010) wrote an interactive procedure within the pipeline which allowed for a better control of each calibration step, we decided to reduce the data manually, using standard IRAF¹ procedures. We started from sci.raw frames and proceeded through object identification, slit extraction, flatfielding, science aperture extraction, lamp aperture extraction, wavelength calibration and normalization of the spectra. Unfortunately, all flat-field images in quadrants 3 and 4 were contaminated by internal reflections. We were forced to substitute the affected image-sections with smooth fits, which, of course, degraded the quality of the corresponding sections of the spectra.

Seven slits produced no useful data. In five cases the target aperture could not be reliably extracted or the spectrum was too noisy, and the catalogued $(B - V)$ values of straggler candidates B283374 and B309015 turned out to be entirely inconsistent with their spectra, suggesting that those objects were either misidentified or very tightly blended. As a result, our sample shrunk to 19 photometric variables and 55 straggler candidates listed in Table A.1. For each of them we obtained ten reduced spectra. Three examples of the spectra are shown in Fig. 1. As detailed below, the information about our objects was mainly extracted from H_{β} . The average S/N at H_{β} was for all objects larger than 20. Out of the total of 740 spectra only a few had $S/N < 20$.

¹ IRAF is distributed by the National Optical Astronomy Observatories, which are operated by the AURA, Inc., under cooperative agreement with the NSF.

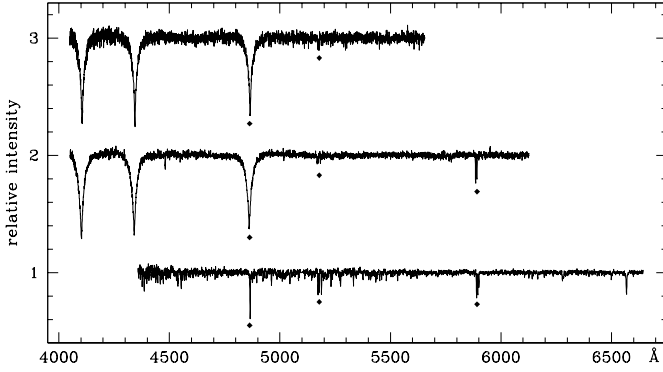


Fig. 1. Three examples of our spectra. The nominal spectral range of VIMOS in the setup used for the present survey begins at 4100 Å, but the recorded spectral range depends on the location of the slit on the mask and may extend shortward of that limit. From top to bottom, shown are: B289620 (shifted upward by 2), B319396 (aka V192; shifted upward by 1) and B155556 (aka V216). Diamonds mark lines used for velocity measurements: H_β at 4861 Å, magnesium triplet at 5167-5184 Å and sodium doublet at 5890-5896 Å.

A broad spectroscopic survey of ω Cen down to $V = 16.5$ mag conducted by van Loon et al. (2007) at a resolution $R \sim 2000$ enabled us to verify the quality of the reduced spectra by a direct comparison. Among 15 of our variables and straggler candidates with $V < 16.5$ we found four in common with their sample. In all four cases the agreement was good – an example is shown in Fig. 2. Note that the nominal spectral range of VIMOS in the setup used for our observations starts at 4100 Å while the spectra of van Loon et al. (2007) extend from 3840 Å to 4940 Å, so that the range covered by both surveys is only 840 Å long.

3. Analysis and results

The actual spectral range recorded by VIMOS depends on the location of the slit on the mask. In our data common to all slits was the region between 4700 and 5600 Å which in many spectra contained practically no lines except H_β and magnesium triplet at 5167.32, 5172.68 and 5183.60 Å (in the hottest objects even the latter was practically undetectable). The sodium doublet at 5889.95 and 5895.92 Å fell beyond the red end of 11 spectra, and H_α was visible in just 13 spectra. As one can see, the material for radial velocity measurements was highly diverse. Moreover, the accuracy of wavelength calibration rapidly deteriorated below 4500 Å, where only two lamp lines (He 4471.48 Å and He 4026.19 Å) were available. Keeping this in mind and aiming to make our survey as uniform as possible, we decided to base the measurements on H_β fitting, using other means for checkup only.

The velocity was measured with the help of the IRAF task SPLIT by fitting Voigt profiles to H_β . Wherever possible, it was also measured the same way from Mg and Na lines. For each line the object’s velocity was calculated as a mean

$$\bar{v} = \frac{1}{N} \sum_{i=1}^N v_i, \quad (1)$$

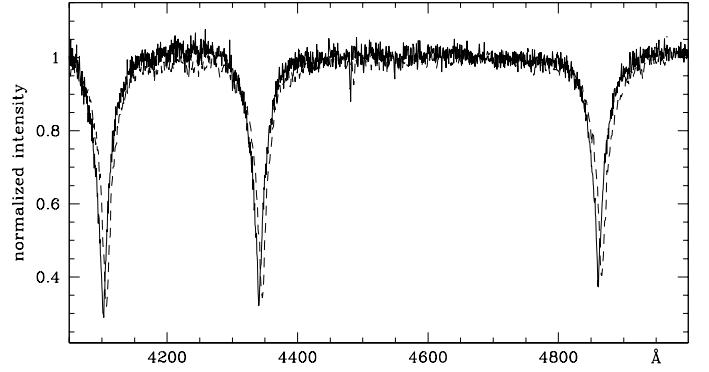


Fig. 2. A test of the quality of our spectra. Shown is the segment of the spectrum of B319396 (aka V192) common to the present survey (solid line) and that of van Loon et al. (2007) (broken line, shifted longwards by 5 Å for clarity). Visible are H_δ , H_γ and H_β .

where $N \leq 10$ is the number of fitted spectra, and the corresponding rms deviation

$$\sigma = \sqrt{\frac{1}{N} \sum_{i=1}^N (\bar{v} - v_i)^2} \quad (2)$$

was found. In the following, velocities and rms deviations are subscripted with the symbol of the element from which they are obtained; e.g. \bar{v}_H or σ_{Na} . The results of sodium-based measurements are further differentiated by indices referring to the origin of the line; e.g. $\bar{v}_{Na,i}$ and $\bar{v}_{Na,s}$ are velocities obtained, respectively, from interstellar and stellar component of the line.

We also attempted to measure the velocities with the help of the IRAF task FXCOR. The measuring procedure consisted of the following steps:

- Based on the recent calibration of Casagrande et al. (2010), the temperature T of each object was estimated from the dereddened $(B - V)$ index assuming $E(B - V) = 0.08$ (McDonald et al. 2009).
- T was rounded to the nearest multiple of 250 K, and a corresponding template from the library compiled by Munari et al. (2005) was assigned to the object. Both $\log g$ and $[Fe/H]$ were the same for all templates and equal to 4.0 and -1.5, respectively.
- Each observed spectrum of the object was cross-correlated with the object’s template.

The second step may seem oversimplified because of the large chemical composition spread in ω Cen (e.g. Johnson & Pilachowski 2010) and obvious spread of gravitational acceleration across our sample, in which V varies by as much as 1.5 mag at constant $B - V$. Also, the empirical formula of Casagrande et al. (2010) loses validity for $(B - V) < 0.19$, i.e. for the eight hottest among our objects, and it may not be applicable to the 14 coolest objects lying far to the right of the main sequence. However, we checked on several objects that reasonable changes in $[Fe/H]$, $\log g$ or even T (i.e. by ± 0.5 dex, ± 0.5 dex, and ± 250 K, respectively) did not modify the results of velocity measurements in any significant way.

The spectral region selected for cross-correlation was located between H_β and sodium doublet (including H_β or more hydrogen lines resulted in extremely broad correlation peaks for hotter objects, whereas including sodium doublet introduced a signal

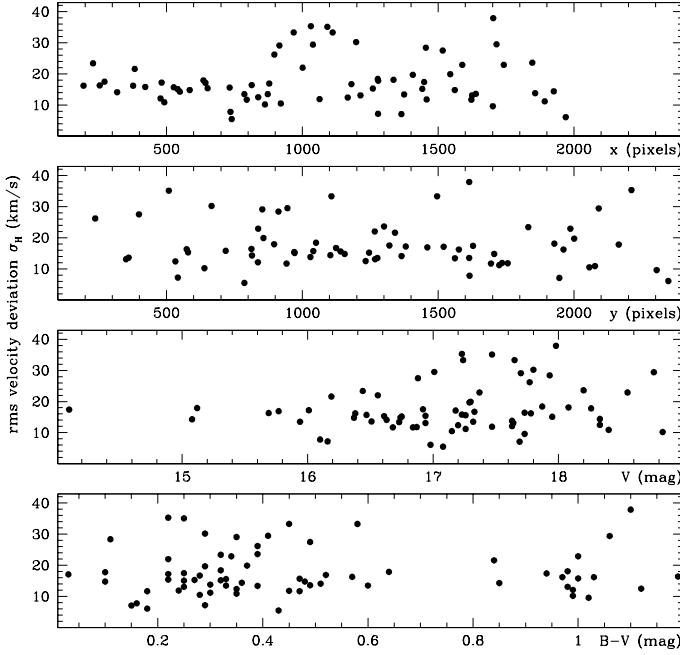


Fig. 3. Results of velocity measurements based on H_β fitting. The rms velocity deviation from the mean velocity of each object is plotted as a function of (x,y) coordinates on the VIMOS mask, object's V -magnitude and object's color. Three objects with $\sigma_H > 40 \text{ km s}^{-1}$ are not shown in order to better visualize the lower rms-range.

from strong interstellar lines). It always contained the magnesium triplet, and its extent was chosen so as to maximize the correlation peak. Because in many hotter spectra the magnesium lines were not very much stronger than the noise, the resultant velocity measurement was considered satisfactory only if the maximum value of the correlation function f_m^c exceeded 0.2 (for the synthetic template cross-correlated with itself f_m^c was equal to 0.8).

3.1. Discussion of errors

H_β was fitted in all spectra of all objects, yielding 74 mean velocities \bar{v}_H and 74 corresponding rms deviations σ_H . The latter originate from inaccurate fitting and/or calibration, and, in the case of binary systems, from the orbital motion. We checked that σ_H does not correlate with object's magnitude or color, nor with the location of the corresponding slit on the VIMOS mask (Fig. 3). This allows us to assume that fitting and calibration errors are purely random with the same Gaussian distribution for all objects:

$$p(x) = \frac{1}{\sqrt{2\pi}s^2} \exp\left(-\frac{x^2}{2s^2}\right), \quad (3)$$

where s is the (yet unknown) standard error of a single H_β -measurement. Then our observable σ_H is obtained by randomly drawing ten values from the distribution (3), and calculating the root mean square:

$$\sigma_H = \sqrt{\frac{1}{10} \sum_{i=1}^{10} x_i^2}. \quad (4)$$

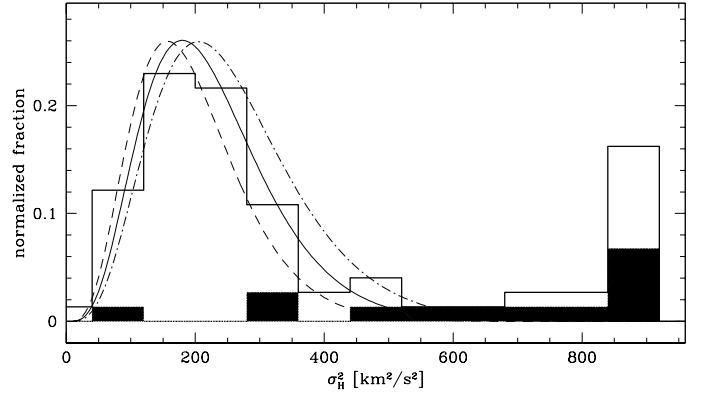


Fig. 4. Histogram of squared rms velocity deviations obtained from H_β fitting. Shaded are photometric variables with periods shorter than 3 d. The expected distributions resulting from equation (5) for $s = 14, 15$ and 16 km s^{-1} , where s is the standard error of a single measurement, are shown with dashed, solid, and dot-dashed line, respectively. The rightmost bar contains all objects with $\sigma_H > 29 \text{ km s}^{-1}$.

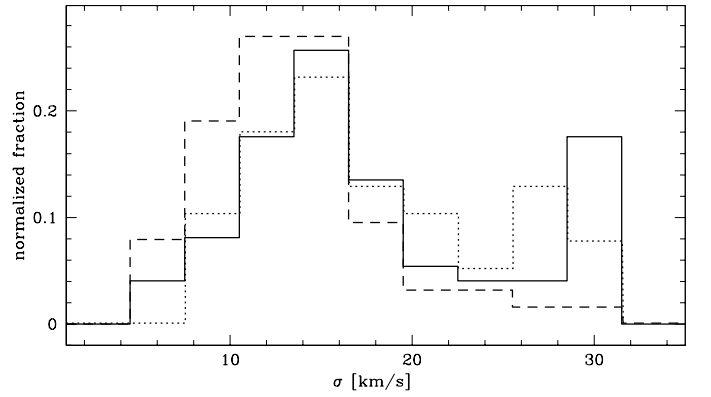


Fig. 5. Histograms of rms velocity deviations σ_H (solid), $\sigma_{\text{Na},i}$ (dashed) and σ_{Mg} (dotted). The rightmost bar of each histogram contains all objects with $\sigma > \sim 29 \text{ km s}^{-1}$. $\sigma_{\text{Na},i}$ measurements are based on the interstellar D_2 line.

The expected distribution of the variable $y \equiv \sigma_H^2$ is chi-square with ten degrees of freedom:

$$p(y) = \frac{26.042}{s^{10}} \exp\left(-\frac{5y}{s^2}\right) y^4. \quad (5)$$

In Fig. 4 the histogram of y obtained from our measurements is compared to distributions (5) with $s = 14, 15$ and 16 km s^{-1} . One can see that for $\sigma_H^2 < \sim 400 \text{ km}^2 \text{ s}^{-2}$ the observed distribution is quite similar to the expected ones, and the high-velocity tail, clearly visible in the histogram but entirely absent from the expected distributions, is largely populated by short-period binaries. These two observations indicate that the assumptions about random nature of H_β -measurement errors and universality of their distribution are entirely reasonable. Among the three fits to the histogram the best one is that with $s = 15 \text{ km s}^{-1}$. Thus, we find that the standard error Δv_H of a single velocity measurement based on H_β fitting is equal to $15 \pm 0.5 \text{ km s}^{-1}$. A similar accuracy of velocity measurements from VIMOS spectra ($10 - 20 \text{ km s}^{-1}$) was reported by Giuffrida et al. (2010). Quantitatively the same, but intuitive rather than rigorous estimate of Δv_H follows from Fig. 5, in which the histogram of σ_H peaks at $\sim 15 \text{ km s}^{-1}$.

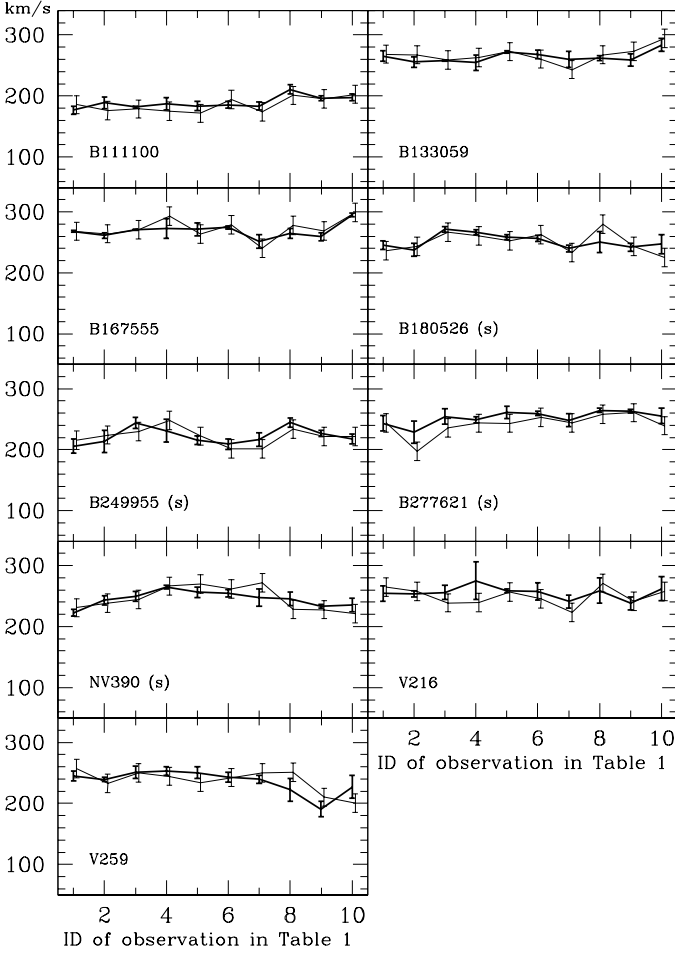


Fig. 6. Velocities obtained from H_β fitting (thin lines) compared to averages v_4 defined by equation (6). Heavy errorbars are rms deviations from v_4 . Thin errorbars (shifted by 0.1 to the right for clarity) mark the standard error of a single H_β measurement estimated in Sect 3.1 (15 km s^{-1}). Objects suspected of being velocity-variable (see Sect. 3.2) are indicated with (s). All velocities are given in the heliocentric frame.

The stellar Na doublet was usually blended with the interstellar one in such a way that the velocity could be reliably measured only from interstellar D_2 and stellar D_1 line (see also van Loon et al. 2007). The interstellar line was measured in all 63 objects whose spectra included the Na doublet, yielding the histogram of $\sigma_{\text{Na},i}$ shown in Fig. 5. By analogy with the histogram of σ_H , its central value of $\sim 13 \text{ km s}^{-1}$ is a good estimate of the standard error of a single velocity measurement based on that line. It is slightly smaller than Δv_H because hydrogen lines are very broad in most objects, which results in increased fitting errors. Also, the wavelength calibration is on the average slightly less accurate at H_β than at the Na doublet because there are fewer lamp lines in the bluer part of the spectrum.

Velocity measurement from magnesium lines was possible for only 39 objects. In nearly all of them the best visible was MgI 5183.6 \AA . Unfortunately, for some objects even that line could not be well fitted in all spectra, so that their \bar{v}_{Mg} and σ_{Mg} had to be calculated from as few as four spectra. As a result, the number of chi-square degrees of freedom was not well determined for the σ_{Mg} observable. Because of that, the histogram of σ_{Mg} in Fig. 5 is not directly comparable to the remaining two histograms. It

was plotted for illustrative purpose only, and the rms deviations σ_{Mg} were not used for further analysis. We only used the mean velocities \bar{v}_{Mg} to check if they differ from their \bar{v}_H counterparts. No systematic differences were found, and the mean difference was equal to just 5.3 km s^{-1} , which confirmed the reliability of mean-velocity measurements based on H_β .

The FXCOR measurements fulfilled the reliability criterion $f_c^m > 0.2$ in the case of 28 objects, while the stellar Na D_1 was strong enough for successful fitting in only 11 objects. As a result, there were just 9 objects for which we collected four complete independent velocity measurements (from H_β , Mg and stellar Na fitting, and from FXCOR). For each spectrum of those objects we calculated the average

$$v_4 \equiv 0.25(v_H + v_{\text{Mg}} + v_{\text{Na},s} + v_{\text{FXCOR}}) \quad (6)$$

and the corresponding rms deviation σ_4 . Fig. 6 shows that there are no significant differences between v_4 and velocities obtained from H_β fitting, thus proving the reliability of the latter. All deviations σ_4 except one range between 2 and 20 km s^{-1} .

We note that FXCOR returns formal velocity errors, but they are correct only to within a scaling factor which depends on the number of counts in the spectra and the Fourier filter parameters used (see e.g. For et al. 2010). For most of our objects they turned out to be unrealistically small ($\sim 2 - 5 \text{ km s}^{-1}$).

3.2. Velocity variables

Fig. 4 suggests that the lower limit of σ_H for the detection of radial-velocity (rv) variables is $\sim 20 \text{ km s}^{-1}$. With this in mind, we checked if the velocities of 11 photometric variables with $\sigma_H > 20 \text{ km s}^{-1}$ are compatible with their lightcurves. To that end we fitted the velocity data of each variable with a sinusoid using its photometric period P_{phot} taken from Kaluzny et al. (2004). The only exception was V379: for this object a period of $0.5P_{\text{phot}}$ was used, which is justified given the ambiguity of the lightcurve of Kaluzny et al. (2004).

The fitting was nearly successful - for the total of 110 points only three departed from the fits by more than $3\Delta v_H$ (two for NV337 and one for V208; see Fig. 7). In particular, we recovered velocity variations of our test-bed object - the V209 system, for which we had independent velocity data provided by Kaluzny et al. (2007a). From the fit in Fig. 7 we find that the velocity semiamplitude of V209 is 32.5 km s^{-1} , which well matches the value of 30.7 km s^{-1} given by Kaluzny et al. (2007a) for the semiamplitude of the primary component (note that the primary is four times brighter than the secondary, so that the contribution of the secondary to our spectra is rather unimportant).

Based on Figs. 4, 5 and 7 we conclude that objects with $\sigma_H > 20 \text{ km s}^{-1}$ may be rather safely identified as genuine rv-variables. Among straggler candidates without light-curves we found 11 such objects which makes a total of 22 rv-variables in the whole sample. Out of them six satisfied the $f_c^m > 0.2$ criterion (four photometric variables and two straggler candidates), and in all those cases the results from FXCOR confirmed the rv-variability found from line fitting. Additionally, we found 17 straggler candidates with $f_c^m > 0.2$ showing consistent velocity variations whose full amplitude exceeded 30 km s^{-1} , which we consider suspected rv-variables (see Table A.1).

3.3. Radial-velocity membership

Using the IRAF task RVCORRECT we transferred the velocities \bar{v}_H to the heliocentric frame. Their histogram is shown in Fig.

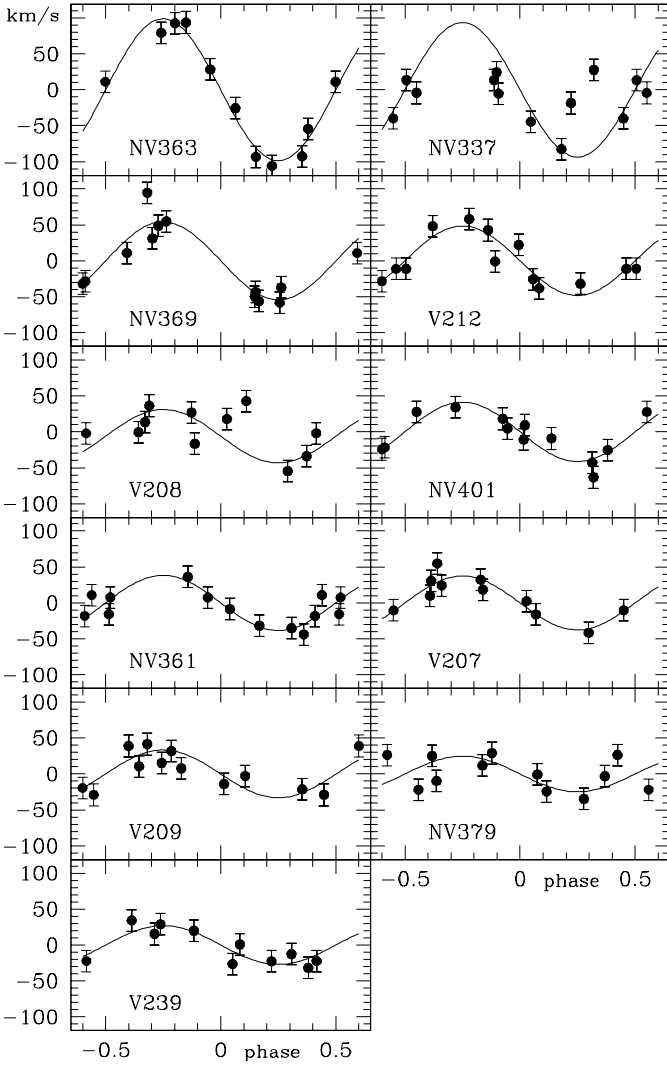


Fig. 7. Radial velocity curves of photometric variables. For each variable the observational data (points) are phased with the corresponding photometric period P_{phot} taken from Kaluzny et al. (2004). The only exception is NV379, where a period of $0.5P_{phot}$ was used for phasing. Smooth curves are sinusoidal fits. Zero points on vertical axes correspond to systemic velocities. The standard error of velocity measurement, estimated in Sect. 3.1, is 15 km s^{-1} .

8a, where we compare it with the histogram of velocities measured for over 1500 stars in the field of ω Cen by van Loon et al. (2007). Before comparison a constant value of -6.2 km s^{-1} was subtracted from the latter to account for the difference between the systemic velocity found by those authors (238.3 km s^{-1}) and the value of 232.1 km s^{-1} given recently by Harris (2010).²

van Loon et al. (2007), who used an instrument with the field of view served by two independent CCDs, found that on one of them the mean velocity of all stars v^* was $\sim 9 \text{ km s}^{-1}$ larger than on the other. They corrected for this effect by lowering all radial velocities from the first CCD by 4 km s^{-1} and by increasing all radial velocities from the second one by an equal amount. Expecting similar problems with our four CCDs, we performed

² The comparison is allowable because our field of view and the central part of their field of view coincide, and the standard error of \bar{v}_H , equal to $\Delta v_H / \sqrt{10}$, is comparable to the velocity error reported in their survey (~ 5 vs. $\sim 8 \text{ km s}^{-1}$).

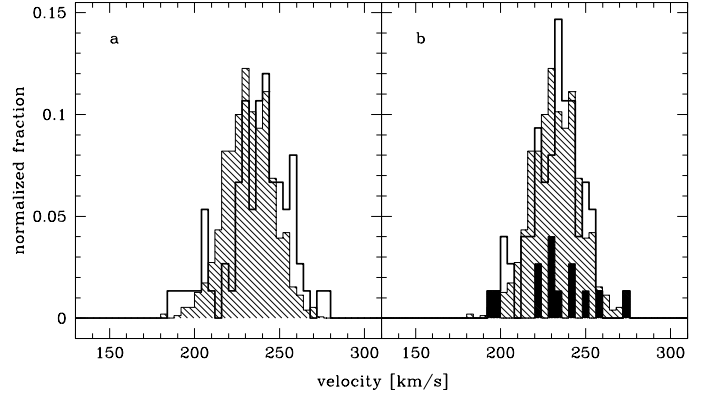


Fig. 8. Histograms of heliocentric \bar{v}_H velocities (heavy line) compared to the histogram of velocities obtained by van Loon et al. (2007) (shaded). a: \bar{v}_H uncorrected; b: \bar{v}_H corrected in such a way that the mean velocity of all objects in each VIMOS quadrant is equal to 232.1 km s^{-1} given recently by Harris (2010) as the systemic velocity of ω Cen. Black bars in Fig. b indicate red straggler candidates.

the same test. Upon averaging \bar{v}_H from Table A.1 over all stars in each quadrant we obtained $v_1^* = 222.5$, $v_2^* = 235.5$, $v_3^* = 238.7$ and $v_4^* = 253.1 \text{ km s}^{-1}$, respectively, for quadrants 1 – 4. To account for these differences, we introduced corrections

$$\Delta v_i^* \equiv v_{sys} - v_i^*, \quad (7)$$

where v_{sys} is the systemic heliocentric velocity of ω Cen equal to 232.1 km s^{-1} (Harris 2010), and i numbers the quadrants. We obtained $\Delta v_{1-4}^* = 9.4, -3.4, -6.6$ and -21.0 km s^{-1} .

The histogram of corrected velocities is shown in Fig. 8b, from which it is evident that our correction procedure makes sense. What remains to be explained are large velocity deviations in quadrants 1 and 4. Possible explanations include mask flexures (although one would expect their effect to be stochastic rather than systematic) and shifts in zero-point velocity caused by differences in optical paths of light rays recorded by different CCDs.

The minimum and maximum corrected heliocentric velocity of our targets was equal, respectively, to 195.1 and 272.4 km s^{-1} (minimum and maximum uncorrected velocity was, respectively, 185.4 and 279.6 km s^{-1}). Based on the kinematic criterion of van Loon et al. (2007), who assign to ω Cen all stars with $180 \text{ km s}^{-1} \leq v \leq 300 \text{ km s}^{-1}$, we may say that almost all objects in our final sample do indeed belong to the cluster. The membership is firmly excluded only for NV369 and B304775, whose velocities, not shown in Fig. 8, fall well below 100 km s^{-1} . Note that this conclusion is valid independently of whether we include corrections defined by equation (7) or not.

4. Discussion

The most exciting goal of the present survey – identification of massive low-luminosity members of ω Cen – was not reached. The lack of accurate ephemerides prevented us from repeating the detailed analysis performed on a smaller sample of ω Cen photometric variables by Rozyczka et al. (2010), but no mass function higher than $f_m = 0.22$ was found, and in addition this particular value was obtained for NV369 – the only photometric variable from the sample whose membership was disproved by our analysis. Typical f_m for cluster members was below 0.05,

indicating rather low-mass companions to photometric variables with rv -variations.

For 72 out of 74 objects investigated here our radial velocity measurements confirmed the proper-motion membership of ω Cen determined by Bellini et al. (2009). This conclusion does not depend on whether corrected or uncorrected velocities are used, as in both cases all rv -members fulfill the kinematic membership criterion of van Loon et al. (2007). The two proper-motion members of ω Cen which turned out to be field objects are B304775 ($mp = 100\%$) and NV369 ($mp = 94\%$), whose uncorrected heliocentric velocities were 44 km s^{-1} and 81 km s^{-1} , respectively. On the other hand, the two objects with the lowest proper-motion membership probability, i.e. NV361 ($mp = 64\%$) and NV332 ($mp = 84\%$), turned out to be genuine members of ω Cen. As solely in those four cases both proper-motion and radial-velocity data were needed to firmly establish the status of the object, our results indicate that the proper-motion catalog of Bellini et al. (2009) is highly ($\sim 95\%$) reliable.

We found that 11 out of 19 photometric variables and 11 out of 55 straggler candidates were rv -variables. The possibility that some rv -variable straggler candidates might be single pulsating stars is rather excluded, as velocity variations with $\sigma_H > 20 \text{ km s}^{-1}$ would cause detectable photometric effects for the Kaluzny et al. (2004) survey. Thus, our results indicate the binary nature of 22 objects. In addition, based on cross-correlation of observed spectra with synthetic templates we identified 17 straggler candidates suspected of being rv -variables. All these objects are shown in Fig. 9 on the CMD of ω Cen.

The high percentage of binary systems in the area occupied in Fig. 9 by blue and yellow stragglers allows us to firmly state that merging is not the only way to produce these objects. In fact, it is quite likely that all stars from our sample located in that region are binaries. V192 and V205 at $(B - V, V) = (0.22, 16.56)$, $(0.28, 17.15)$, for which we have not found clear rv -variations, are eclipsing variables (Kaluzny et al. 2004). NV380, NV374 and V259 at $(0.03, 17.18)$, $(0.16, 16.10)$ and $(0.57, 15.69)$ have rather long periods (7.83, 3.31 and 19.12 d, respectively), and may have easily escaped recognition if their orbital inclinations are not close to 90° . If we number them among suspected rv -variables, for the total of 51 cluster members located in the discussed region there will be 33 (i.e. 65%) for which an indication of rv -variability was found. If we additionally include the binary blue stragglers discussed by Rozyczka et al. (2010), this ratio increases to 69%.

Similar fractions of binary blue stragglers were found in two old open clusters: Mathieu & Geller (2009) identified 16 binaries among 21 blue stragglers of NGC 188, and Latham (2007) found 8 binaries among 13 blue stragglers of M67. However, both in NGC 188 and M67 almost all binary blue stragglers have much longer periods than the objects discussed here – typically on the order of ~ 1000 days. Our spectroscopic survey lasted two weeks only, and in addition it was not sensitive to low velocities. As a result, we would not find any long-period variables even if they were there, and the lack of such objects in our sample may be a pure selection effect. However, the small percentage of short periods in NGC 188 and M67 compared to ω Cen is real, and it must have a physical cause. Mathieu & Geller (2009) point out that “the observation of binaries with circular orbits and periods of ~ 1000 d in both NGC188 and M67 indicates that these blue straggler binaries have not been disturbed dynamically since their formation”. It is thus conceivable that the frequency of dynamical interactions in both open clusters is too low to cause efficient tightening of binary orbits, while in ω Cen it might be high enough to produce the observed short-period

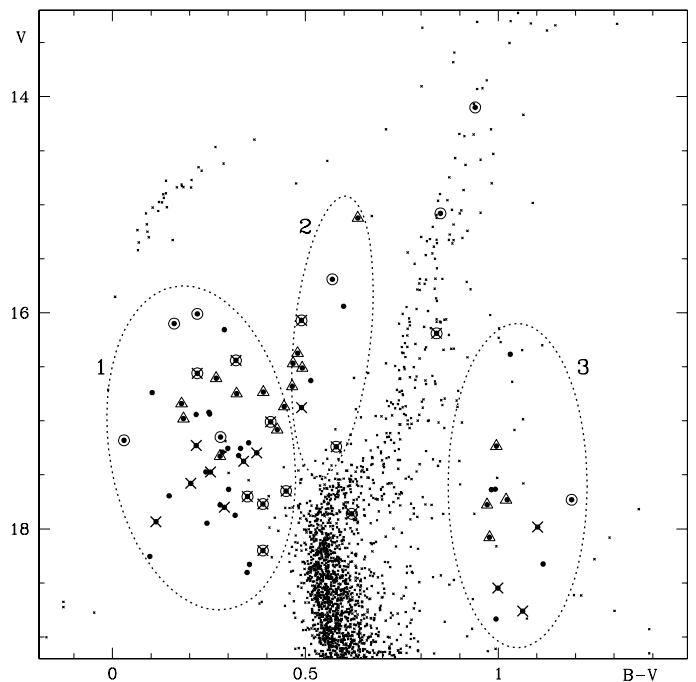


Fig. 9. Location of the investigated objects (large dots) on the CMD of ω Cen. Circles: photometric variables. Crosses: radial-velocity variables. Triangles: suspected radial-velocity variables. Ellipses 1, 2 and 3 indicate approximate locations of regions occupied, respectively, by blue, yellow and red stragglers (see also Sect. 1). The background CM-diagram is from our unpublished photometry of a 2.6×2.6 arcmin field centered at $\alpha = 13^{\text{h}}27^{\text{m}}42^{\text{s}}.2$, $\delta = -47^{\circ}23'34''$, obtained on the 2.5-m duPont telescope at Las Campanas Observatory.

systems. In any case, the fact that binaries are standard members of the blue and yellow straggler population is a strong argument in favor of the hypothesis explaining the origin of these objects by a significant but rather quiet mass exchange in binary systems which rarely, if ever, leads to merging. Our findings support the results of Ferraro et al. (2006), who, based on the flat radial distribution of blue stragglers in ω Cen, ruled out the collisional origin of these objects, and suggested that they are the progeny of primordial binaries. The same conclusion was reached by Dalessandro et al. (2008) in relation to NGC 2419.

Interesting objects have been found also to the right of the main sequence and below the subgiant branch of several clusters. They are the so-called red stragglers or sub-subgiants (e.g. Platais et al. 2011). As remarked by Platais et al. (2011) in relation to NGC6971, “these apparent binary stars occupy an area of the CMD ... which is not easy to populate with any combination of two normal cluster stars.” At least some candidate red stragglers in ω Cen are X-ray sources, however the cause of their X-ray activity remains obscure (Haggard et al. 2010). The two binary red stragglers in M67 studied by Mathieu et al. (2003) may belong to the RS CVn class, but their parameters have not been uniquely determined. Mathieu et al. (2003) and Mathieu (2008) argue that their evolutionary history might have included mass transfer episodes, mergers, dynamical stellar exchanges and/or close encounters leading to envelope stripping. In their conclusion Mathieu et al. (2003) point to an intriguing possibility that these systems are progenitors of blue stragglers.

According to the kinematic criterion of van Loon et al. (2007), who define ω Cen members as those with $180 < v < 300$

km s⁻¹, all the 13 objects from our sample which reside to the right of the main sequence and red giant branch of the cluster, are members of the cluster (to be on the safe side, one may classify the three objects with extreme velocities as “likely members”; see Fig. 8 and Table A.1). 12 red stragglers are sub-giants, but the last one, B167555 at $(B - V, V) = (1.03, 16.38)$, is less luminous by only ~ 0.2 mag than the photometrically and radial-velocity variable red giant NV379 at $(0.84, 16.19)$, so that the alternative term “red straggler” fits it much better. Our red-straggler sample includes up to eight (i.e. up to 62%) binaries: the eclipsing variable NV332 accompanied by rv-variables B253281, B121450 and B146967 and four suspected rv-variables. It is thus conceivable that the remaining 5 objects are also binary systems, which would support the final conjecture of Mathieu et al. (2003). If that conjecture is right then red stragglers are relatively fresh products of complex interactions between cluster members, and as such they may turn out to be even more interesting than the blue stragglers themselves.

5. Conclusions

Our spectroscopic study of 74 proper-motion members of ω Cen confirmed the membership of 72 objects. Among 55 blue stragglers belonging to our sample we found 22 binaries and 13 suspected binaries, whereas among 13 red stragglers we found 4 binaries and 4 suspected binaries. The fact that binarity is normal in these intriguing populations leads one to expect that their evolutionary conundrums will be solved once good light-curve and velocity-curve solutions are found. We hope that our results will prompt the relevant photometric and spectroscopic research.

Acknowledgements. Research of JK, PP, MR and WP is supported by the grant MISTRZ from the Foundation for the Polish Science and by the grants N N203 379936 and N N203 301335 from the Polish Ministry of Science and Higher Education. Support for MC and CC is provided by the Ministry for the Development, Economy and Tourism Programa Inicativa Cientifica Milenio through grant P07-021-F, awarded to The Milky Way Millenium Nucleus; by Proyecto Basal PFB-06/2007; by FONDAPE Centro de Astrofísica 15010003; and by Proyecto FONDECYT Regular #1110326. We are sincerely grateful to the anonymous referee whose detailed suggestions greatly improved the quality and the exposition of the paper.

References

- Bates B., Wood K. D., Catney M. G. & Gilheany S., 1992, MNRAS, 254, 221
 Bellini, A., Piotto, G., Bedin, L. R., et al., 2009, A&A, 493, 959
 Calamida, A., Stetson, P. B., Bono, G. et al., 2005, ApJ, 634, L69
 Casagrande, L., Ramírez, I., Meléndez, J., Bessell, M. & Asplund, M., 2010, A&A, 512, A54
 Dalessandro, E., Lanzoni, M., Ferraro, F. R. et al., 2008, ApJ, 681, 311
 ESO, 2011, online document at www.eso.org/observing/dfo/quality/VIMOS/ServiceMode/ServiceMode.html
 Ferraro, F. R., 2006, arXiv:astro-ph/0601217v1
 Ferraro, F. R., Sollima, A., Rood, R. T. et al, 2006, ApJ, 638, 433
 For, B.-Q., Green, E. M., Fontaine, G. et al., 2010, ApJ, 708, 253
 Giuffrida, G., Sbordone, L., Zaggia, S. et al., 2010, A&A, 513, A62
 Haggard, D., Cool, A. M., Arias, T. et al., 2010, AIPC, 1314, 157
 Harris, W. E., 2010, arXiv:1012.3224
 Johnson, C. I. & Pilachowski, C. A., 2010, ApJ, 722, 1373
 Kaluzny, J., Olech, A., Thompson, I. B. et al., 2004, A&A, 424, 1101
 Kaluzny, J., Rucinski, S. M., Thompson, I. B., Pych, W. & Krzeminski, W., 2007a, AJ, 133, 2457
 Kaluzny, J., Thompson, I. B., Rucinski, S. M., et al. 2007b, AJ, 134, 541
 Latham, D. W., 2007, Highlights Astr., 14, 444
 Mathieu, R. D., 2008, IAUS, 246, 79
 Mathieu, R. D. & Geller, A. M., 2009, Nature, 462, 1032
 Mathieu, R. D., van den Berg, M., Torres, G. et al., 2003, AJ, 125, 246
 McDonald, I., van Loon, J. Th., Decin L. et al., 2009, MNRAS, 394, 831
 Munari, U., Sordo, R., Castelli, F. & Zwitter, T., 2005, A&A, 442, 1127
 Origlia L., Gredel R., Ferraro F. R. & Fusi Pecci F., 1997, MNRAS, 289, 948

- Platais, I., Cudworth, K. M., Kozhurina-Platais, V. et al., 2011, ApJ, 733, L1
 Pooley, 2010, PNAS, 107, 7164
 Remillard, R. A., & McClintock, J. E. 2006, ARA&A, 44, 49
 Rozyczka, M., Kaluzny, J., Pietrukowicz, P. et al., 2010, A&A, 524, A78
 Sandage, A. R., 1953, AJ, 58, 61
 van Loon, J. Th., van Leeuwen, F., Smalley, B. et al., 2007, MNRAS, 382, 1353
 van Loon, J. Th., Smith, K. T., McDonald, I. et al., 2009, MNRAS, 399, 195
 Verbunt, F., Pooley, D. & Bassa, C., 2008, IAU Symp., 246, 301
 Wood K. D. & Bates B., 1993, ApJ, 417, 572
 Wood K. D. & Bates B., 1994, MNRAS, 267, 660
 Xin, Y., Deng, L., de Grijs, R. & Kroupa, P., 2011, MNRAS, 411, 761

Appendix A: The baffling histogram of ISM velocity

ω Cen is an ideal laboratory to study small-scale structure and dynamics of the interstellar medium (ISM) by using its stars as densely spaced beacons. In fact, within the last two decades there were several such attempts. Bates et al. (1992) and Wood & Bates (1993, 1994) found several components of NaI D₂ at velocities between 0 and -40 km s⁻¹, “with the most conspicuous changes of the line profiles occurring in the most negative components, where variations were seen on an angular scale of ~ 1 arcmin”. Strong patchiness of the absorbing medium was reported by Calamida et al. (2005), who registered “clumpy extinction variations by a factor of almost two across the core of the cluster”. van Loon et al. (2007) detected a *redshifted* component of the CaII K line. Since it was visible only near the centre of ω Cen, they suggested that it originated in a medium located within the gravitational influence of the cluster. High positive velocities were also measured in HI and CO emission lines (Origlia et al. 1997). A detailed mapping of interstellar clouds in front of ω Cen was recently performed by van Loon et al. (2009). They found the ISM to be patchy at all scales from 0.7° (the size of their field) down to about $30''$ (the closest distances between sightlines to sampled stars). The mean heliocentric velocity of the CaII K and NaI D₂ lines obtained from their survey is equal to -24 and -11 km s⁻¹, respectively. The histogram of heliocentric NaI D₂ velocities based on their online data peaks at -11 km s⁻¹, and it is practically limited to the range between -6 and -16 km s⁻¹.

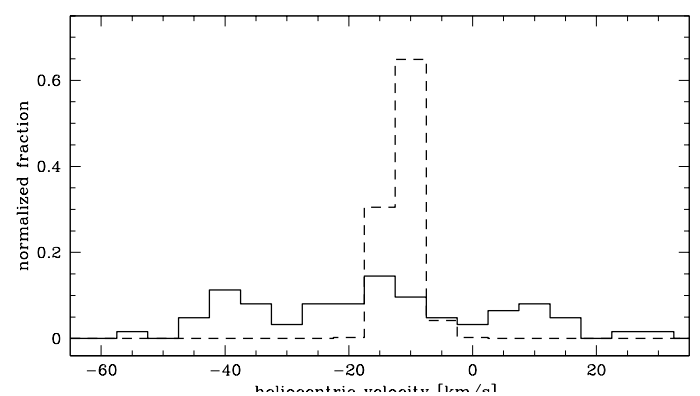


Fig. A.1. Histogram of heliocentric velocities obtained from NaI D₂ line. Solid: our data. Broken: van Loon et al. (2009).

The above brief review indicates that the problem of the ISM in front of ω Cen is far from being solved, and this is what prompted us to extract the relevant information from our data. We measured the velocities of the NaI D₂ line, converted them to the heliocentric reference frame, and added quadrant-dependent

corrections introduced in Sect. 3.3. The resulting velocity histogram, shown in Fig. A.1, turns out to be entirely different from that of van Loon et al. (2009): the central maximum is much lower, broader and shifted by $\sim 5 \text{ km s}^{-1}$ toward more negative velocities. Moreover, an excess of objects with velocities between -35 and -45 km s^{-1} and another one centered around $+10 \text{ km s}^{-1}$ seem to be present.

Unfortunately, we do not have any common objects with van Loon et al. (2009), so that a direct comparison of the spectra is impossible. Errors on our side could originate from wrong velocity measurements, misidentification of spectral lines or bad wavelength calibration. However, for each object \bar{v}_{Na} is an average over ten spectra. If true velocities were indeed strongly peaked at -11 km s^{-1} then it would be difficult to imagine how such mean values could be wrong by as much as $\sim 30 \text{ km s}^{-1}$ to produce spurious peaks at -40 and $+10 \text{ km s}^{-1}$. Further, the identification of the NaI doublet is so easy that we can entirely exclude it as a source of errors. In hotter stars there are no strong lines with which it could be mistaken, and in cooler stars the doublet turns into a unique triplet composed of interstellar D_2 and stellar D_1 with a blend of interstellar D_1 and stellar D_2 in between (Fig. A.2).

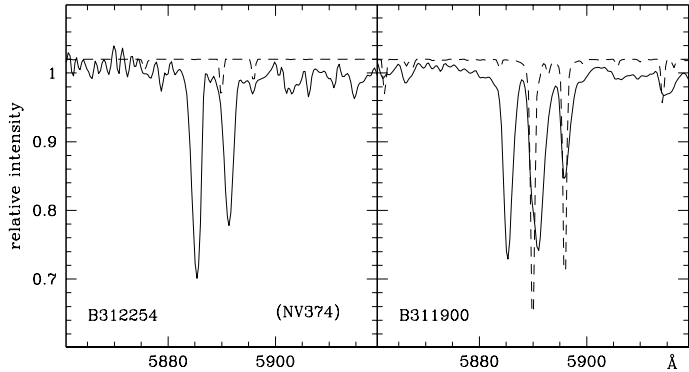


Fig. A.2. NaI doublet in Doppler-corrected spectra of B312254, aka NV374 ($B - V = 0.16$), and B311900 ($B - V = 0.64$). The observed spectra (solid lines) are compared to synthetic templates assigned as explained in Sect. 3.2 (broken lines). The templates are shifted upwards by 0.02 for clarity. Because the stellar spectra have been Doppler-corrected for the velocity obtained from H_β , the ISM components appear shifted with respect to the rest wavelengths.

Shortwards of H_β our wavelength calibration is inaccurate in some objects (ESO 2011), but between H_β and H_α it should be rather correct. We verified this by selecting a few spectra that contain both these lines, Doppler-correcting them for the velocity obtained from H_β , and comparing with the corresponding synthetic templates assigned as explained in Sect. 3.2. In Doppler-corrected spectra H_α fell in the right place, and the stellar D_1 line was also properly placed (Fig. A.2). Note that for a spurious shift of $\sim 30 \text{ km s}^{-1}$ a relatively large calibration error of $\sim 0.3 \text{ \AA}$ is needed which should be easily visible in Doppler-corrected spectra. Of course, smaller wavelength mismatches could have escaped out attention.

Another factor suspected of generating errors is instrumental effects (mask flexures, different zero-point velocities in different quadrants and/or slits). As a result, it might turn out that our velocity corrections introduced in Sect. 3.3 should vary not only between quadrants, but also between slits, and there would be no

way to calculate them. One would have to accept that absolute velocities obtained from blue VIMOS spectra may be wrong by up to $\pm 30 \text{ km s}^{-1}$ (on the other hand, it was shown in Sect. 3.2 that the instrument is stable enough for reliable measurements of velocity variations with an accuracy of $\sim 15 \text{ km s}^{-1}$).

Table A.1. List of objects.

	Bellini	$B - V$	V	VQ	$\bar{v}_{H\beta}$	$\sigma_{H\beta}$	\bar{v}_{Na}	σ_{Na}	Kaluzny	Period	Pvar	Vvar	remark
1	69263	0.36	18.33	1	227.5	12.7	-5.7	9.2					
2	69830	0.30	17.26	4	239.7	12.8	25.4	13.5					
3	81157	0.22	17.23	1	210.6	34.9	-55.7	12.8				v	
4	85380	0.25	16.94	1	230.4	12.4	-50.8	17.1					
5	87731	0.48	16.37	4	254.5	14.0	26.0	14.9					s
6	95154	0.32	16.75	4	256.9	15.9	2.7	6.4					s
7	95702	0.11	17.93	1	191.2	27.6	-49.1	20.7					v
8	99931	0.29	16.16	4	254.5	7.2	34.4	16.4					
9	100977	0.39	16.73	1	239.7	12.0	-43.4	13.7					s
10	107036	0.27	16.61	4	252.0	15.9	11.1	7.5					s
11	107122	0.32	17.87	1	202.9	16.6	-47.0	15					
12	111100	0.98	17.64	1	185.4	11.3	-53.2	7.8					lrs
13	113098	0.35	17.20	4	248.9	13.4	13.5	9.9					
14	114490	0.28	17.78	1	195.6	14.7	-48.8	10					
15	118163	0.45	17.65	1	205.5	32.0	-32.3	11.6	NV337	0.269	EW?	v	
16	121450	1.06	18.76	4	279.6	31.8	0.0	0				v	rs
17	121591	0.24	17.47	1	226.5	10.5	-46.6	16.3					
18	124330	0.49	16.07	1	81.2	66.1	0.0	0	NV369	1.788	?	v	nm
19	130105	0.35	17.70	4	243.2	30.6	9.7	13.9	NV401	0.354	?	v	
20	131682	0.47	16.68	1	197.9	10.2	-52.1	10.7					s
21	133059	0.60	15.94	4	266.9	13.0	16.0	14.3					
22	135321	0.99	18.83	1	232.6	10.4	-20.6	27.3					rs
23	137605	1.19	17.73	4	241.4	17.0	12.7	11.3	NV332	0.247	EW		rs
24	140758	0.33	17.32	1	242.6	12.4	-30.9	10.6					
25	142842	0.33	17.26	4	241.4	30.7	2.4	11.2					
26	143829	0.43	17.08	1	244.3	5.3	-27.1	25.2					s
27	146095	0.20	17.58	4	256.9	64.1	-7.6	11.9				v	
28	146967	1.10	17.98	1	262.7	35.6	13.1	45				v	lrs
29	148727	0.03	17.18	4	246.3	17.4	-4.1	15.8	NV380	7.832	?		
30	149714	0.22	16.94	1	230.5	14.6	-49.7	12					
31	154483	0.10	16.74	1	228.9	13.7	-49.4	9.9					
32	155556	0.85	15.08	4	249.6	13.7	1.2	9.7	V216	23.737	LT		rg
33	157688	0.25	17.95	1	225.6	13.7	-40.4	10.2					
34	159485	0.35	18.40	4	263.9	11.6	0.0	0					
35	162119	0.99	17.63	1	219.7	12.6	-52.8	9.1					rs
36	166068	1.00	17.23	1	233.8	15.2	-49.2	10.7					s
37	167555	1.03	16.38	4	272.3	15.5	15.3	13.9					rs
38	171825	0.51	16.63	4	253.2	14.7	6.4	15.1					
39	176840	0.25	16.92	1	229.2	15.8	-43.7	8.4					
40	177256	0.57	15.69	4	237.3	17.6	-2.4	9	V259	19.120	sp?		
41	179912	0.32	16.44	1	229.8	23.0	0.0	0	V239	1.189	EA	v	
42	180526	0.97	17.78	4	250.4	16.2	-35.0	11.6					s
43	234296	0.15	17.69	3	251.2	7.8	0.0	0					rs
44	234998	0.39	18.20	2	237.4	24.5	-2.1	15.5	NV361	0.682	EA	v	
45	241994	0.30	17.63	3	227.8	14.0	7.3	17.5					
46	244408	0.41	17.01	2	248.0	28.9	-12.3	14.8	V208	0.306	EW	v	
47	249955	0.49	16.51	2	222.0	13.4	-13.9	15.7					s
48	250383	0.34	17.37	3	255.4	21.5	0.0	0					v
49	253226	1.02	17.73	3	237.8	9.3	0.0	0					s
50	253281	1.00	18.55	2	225.2	22.1	-24.0	25.4					v
51	258274	0.49	16.88	2	206.9	27.0	-21.3	17.3					v
52	258539	0.18	16.84	3	241.0	10.8	19.3	8.4					s
53	262766	0.94	14.10	2	246.1	18.4	-11.3	22	NV390	15.710	?	s	rg
54	263560	0.37	17.30	3	207.3	18.4	9.8	14.3					v
55	265591	0.29	17.29	2	219.1	19.7	0.0	0					
56	269775	0.45	16.87	3	235.7	11.5	17.4	8					s
57	274338	0.18	16.98	2	237.3	6.8	-13.1	17					s
58	277621	0.98	18.08	3	241.9	16.7	-27.6	10.2					s
59	279427	0.29	17.80	2	239.7	30.5	31.7	16.7					v
60	281267	0.10	18.26	3	259.5	17.5	0.0	0					

Table A.1. continued.

	Bellini	$B - V$	V	VQ	\bar{v}_H	σ_H	\bar{v}_{Na}	σ_{Na}	Kaluzny	Period	Pvar	Vvar	remark
61	287148	0.28	17.33	3	230.0	15.0	16.0	11.2					s
62	289620	0.25	17.47	2	256.7	34.1	0.0	0					v
63	293439	0.58	17.24	2	243.9	31.9	-7.7	16.9	V212	2.467	EA		v
64	297708	0.39	17.77	2	238.5	26.6	-18.1	14.5	V207	0.276	EW		v
65	297731	0.22	16.56	3	256.5	22.6	15.7	11.3	V209	0.834	EA		v
66	302520	0.28	17.15	3	230.9	8.6	0.0	0	V205	0.369	EA		
67	304775	0.52	15.77	3	44.4	15.9	35.0	8.9					
68	306843	1.12	18.33	3	206.0	14.8	23.0	6.5					nm lrs
69	311900	0.64	15.12	2	228.5	17.0	-11.9	11.1					s
70	312254	0.16	16.10	3	246.7	15.1	18.3	6.7	NV374	3.311	?		
71	317269	0.47	16.47	2	240.6	14.5	-11.6	14					s
72	319396	0.22	16.01	2	241.9	17.0	-12.7	11.1	V192	1.376	EA		
73	321474	0.62	17.86	3	256.6	74.6	7.5	16.4	NV363	0.824	EA		v to
74	328605	0.84	16.19	3	233.8	19.8	14.9	6.9	NV379	7.104	?		v rg

Legend:

Bellini - object's number in Bellini et al. (2009).

$B - V$ - color index, not corrected for reddening.

V - V -band magnitude.

VQ - number of VIMOS quadrant.

\bar{v}_H and σ_H - mean value and rms deviation of velocity calculated from $H\beta$.

\bar{v}_{Na} and σ_{Na} - mean value and rms deviation of velocity calculated from the interstellar NaI D₂ line (0 if the spectrum did not reach to the NaI doublet).

Kaluzny - object's number in Kaluzny et al. (2004).

Period - photometric period in days.

Pvar - type of photometric variability after Kaluzny et al. (2004): EA = Algol; EW = W UMa; LT = long term; SP = spotted.

Vvar - flag for velocity variability: v = variable; s = suspected.

Remarks: rs = red straggler; lrs = likely red straggler; rg = red giant; to = turnoff object; blank - object located to the left of main sequence and red giant branch (blue straggler, yellow straggler or hot subdwarf).

The velocities are given in the heliocentric frame without corrections described in Sect. 3.3. The values of the corrections are 9.4, -3.4, -6.6 and 21.0 km s⁻¹ for quadrants 1 – 4, respectively.